Tensile, Edgewise Bending, Flatwise Bending, and Non-Destructive Evaluations of Visually Graded Fir Boards

Fatih Kurul *

Tensile, edgewise, and flatwise bending behaviors of visually graded fir (*Abies nordmanniana* subsp. *bornmuelleriana*) boards were investigated through destructive and non-destructive testing to evaluate their mechanical performance and grading accuracy. A total of 724 specimens were prepared and tested in accordance with EN 408 standards. Knot diameter ratios (narrow, mean, and parallel) were used to establish three visual grading methods. Vibration-based (PLG, Hitman) and time of flight (ToF) (Microsecond Timer, Ultrasonic Timer, and Sylvatest Duo) techniques were used for non-destructive evaluation (NDE), along with screw withdrawal tests. The results showed that although the vibration method had lower dynamic modulus of elasticity (MOEd) values than the ToF method, it provided stronger correlations with tensile and bending properties. The mean and parallel knot diameter ratios provided more reliable grading results than the narrow ratio. Tensile strength was more affected by defects than bending strength, and the flatwise bending method consistently produced the highest strength values. The adjustment from global to local MOE reduced modulus values below 9000 MPa, resulting in lower strength class assignments. Overall, the vibration-based NDE method proved the most effective for predicting lumber quality, and the flatwise bending test emerged as a viable alternative to tension and edge bending methods for structural grading.

DOI: 10.15376/biores.21.1.1364-1387

Keywords: Knot diameter ratio; Visual grading; Fir; Vibration; Time of flight; Screw withdrawal

*Contact information: Istanbul University-Cerrahpaşa Faculty of Forestry, Department of Wood Mechanics and Technology, Istanbul, Türkiye; *Corresponding author: fatihkurul@iuc.edu.tr*

INTRODUCTION

Wood has long been recognized as one of the most sustainable and versatile materials in structural engineering applications. Its renewability, favorable density/strength ratio, and natural aesthetic appeal have made it a building material used for centuries (Ridley-Ellis *et al.* 2016; Kurul and As 2024). Today, wood, which remains essential in modern engineering and architecture, is gaining attention as an alternative to steel and concrete as sustainability becomes a key issue in construction. Beyond its positive aspects, wood is also a complex engineering material that requires careful attention due to its wide variation in physical and mechanical properties, driven by its natural structure and inherent imperfections (Kurul and As 2024; Kurul *et al.* 2024). Therefore, intensive research is being conducted on its mechanical behavior and performance under various loading conditions (Stapel and van de Kuilen 2014; Ridley-Ellis *et al.* 2016; Kurul *et al.* 2025).

In Europe, a series of standards published by the European Committee for Standardization (CEN) is used to ensure quality control and form the basis for design calculations in the use of wood for structural purposes (Ridley-Ellis *et al.* 2016). These standards form the basis for visual and mechanical strength grading of wood structural materials, enabling their safe and economical use in construction. The application of grading systems for wood structural materials is essential not only for quality control but also for the reliability of engineering calculations (Steiger and Arnold 2009; Ridley-Ellis *et al.* 2016; Kurul and As 2024). The standard EN 1995-1-1 (2023) (Eurocode 5) stipulates that the strength values of wood used in structural system designs should be determined according to the classes specified in EN 338 (2020). The EN 338 (2020) standard includes three systems: "C and D" classes obtained from edgewise bending tests, and "T" classes obtained from tensile tests. While structural grading in Europe is primarily based on edgewise bending tests, tensile properties are equally important, especially for elements such as glulam lamellas (Gil-Moreno *et al.* 2022). Countries participate in this system by subjecting tree species to visual or machine strength classification, and the results are published in the EN 1912 (2024) standard.

Visual grading is a traditional quality assessment method based on measuring the physical defects of timber, such as the slope of grain, knot diameters, fissures, wane, and resin pockets (Seco *et al.* 2004; Stapel and van de Kuilen 2013; Stapel and van de Kuilen 2014; Ridley-Ellis *et al.* 2016; Kurul *et al.* 2024; Kurul and As 2024; Kurul 2025). While each country has its own visual grading criteria, the EN 14081-1 (2019) standard specifies lower limit values for these defects. All local standards must meet the lower limit values specified in this standard (Steiger and Arnold 2009; Ridley-Ellis *et al.* 2016). Visual grading methods provide a cost-effective and straightforward assessment. However, their main disadvantage is their reliance on human observation and experience (Brunetti *et al.* 2016; Kurul and As 2024). Machine grading, performed using non-destructive devices that automatically measure some mechanical and physical properties of wood, is considered a more objective and repeatable method (Steiger and Arnold 2009; Nocetti *et al.* 2010; Ridley-Ellis *et al.* 2016; Ravenshorst and van de Kuilen 2016; Kurul and As 2024). This method typically uses parameters, such as stress wave velocity, vibration frequency, or flexural modulus, to estimate the timber's strength class (Arriaga *et al.* 2012; Brunetti *et al.* 2016; Gil-Moreno *et al.* 2022). The machine classification process, according to European standards, is defined in EN 14081-2 (2018).

Accurately identifying natural defects within wood is important for visual and machine strength grading. The measurement principles for all defects in wood materials intended for structural use are outlined in EN 1309-3 (2018). Knots are among the most critical natural growth defects in wood construction materials and are a key factor directly affecting timber's mechanical strength (As *et al.* 2006; Roblot *et al.* 2010; Guindos and Guaita 2014). Studies have shown that knot ratio, knot diameter, knot area, and location are decisive factors in the impact of knots on wood strength. Furthermore, it has been determined that as the knot diameter increases, the wood's bending and tensile strengths, as well as the bending and tensile modulus of elasticities, decrease significantly (As *et al.* 2006; Roblot *et al.* 2010; Guindos and Guaita 2014; Qu *et al.* 2020; Lovrić Vranković *et al.* 2025). Therefore, knot diameter or knot area measurements are among the most important criteria for determining the visual grade of lumber in national visual classification standards.

Many studies conducted in Europe have determined the visual and mechanical strength classes of structural boards, classified using both destructive and non-destructive methods. The majority of these studies have been based on edgewise bending tests (Fink

and Kohler 2011; Krajnc *et al.* 2019; Rais *et al.* 2021; Kurul *et al.* 2024; Kurul 2025; Lovrić Vranković *et al.* 2025). However, few studies have simultaneously examined the tensile, edgewise, and flatwise bending strengths of wood using both destructive and non-destructive methods. This study aims to compare and correlate the tensile, edgewise bending, and flatwise bending tests of visually graded fir structural boards using three methods to determine the knot diameter ratio (KDR). With this, the aim is to select the best method by examining three methods for measuring KDR. In this context, C and T classes were separately calculated and compared for each quality class determined by the three KDR methods for three different tests. In addition, the research aimed to correlate destructive tests with non-destructive tests (screw withdrawal, stress wave method using three separate devices, and vibration methods using two separate devices) to estimate wood quality as accurately as possible and to determine which devices were most efficient. Finally, 3-point and 4-point bending tests were performed on small-clear specimens to determine and compare the bending characteristics of the fir species. Thus, it was planned to increase the usage potential of the fir species, which is suitable for use in engineered structural wood materials and an important raw material source for the regional industry, by examining the structural characterization of the most commonly used destructive and non-destructive methods.

EXPERIMENTAL

Wood Specimens

In this study, 80 samples of fir (*Abies nordmanniana* subsp. *bornmuelleriana*) with dimensions of 30 x 210 x 4000 mm³ (thickness × width × length) were used. The wood pieces were supplied by a commercial firm and dried to 12% (±2) moisture content. These samples were initially cut as shown in Fig. 1. The evaluations included a tensile test (A1-B2), an edgewise bending test (A2-B1), a flatwise bending test (C1-C2), and 3- and 4-point small-clear bending test samples (D1-D2-D3); a total of 724 test samples were prepared (Fig. 2). The moisture content of all samples was then measured using an electrical resistance method, as described in EN 13183-2 (2002) (Fig. 3). The sample code, group no, test type, dimension, number of samples and average moisture content for each test group are given in Table 1.

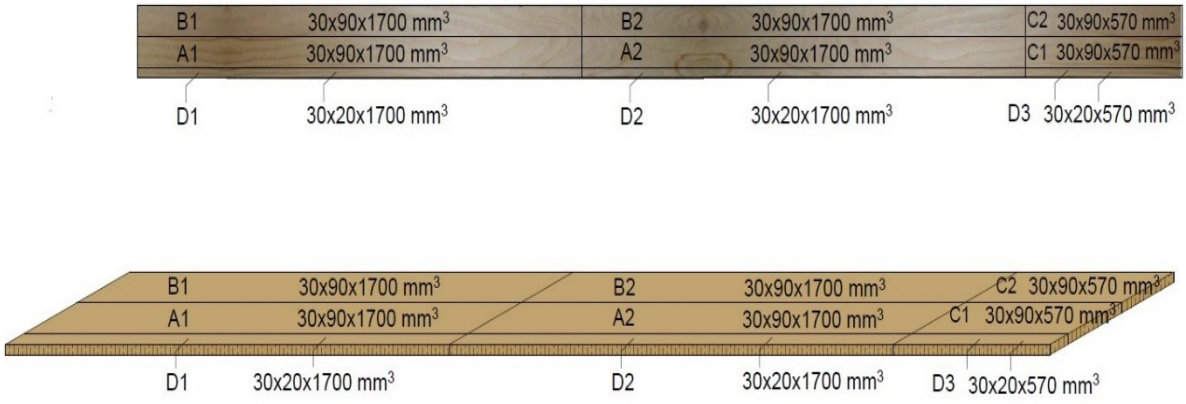

Fig. 1. Cutting diagram of fir structural boards

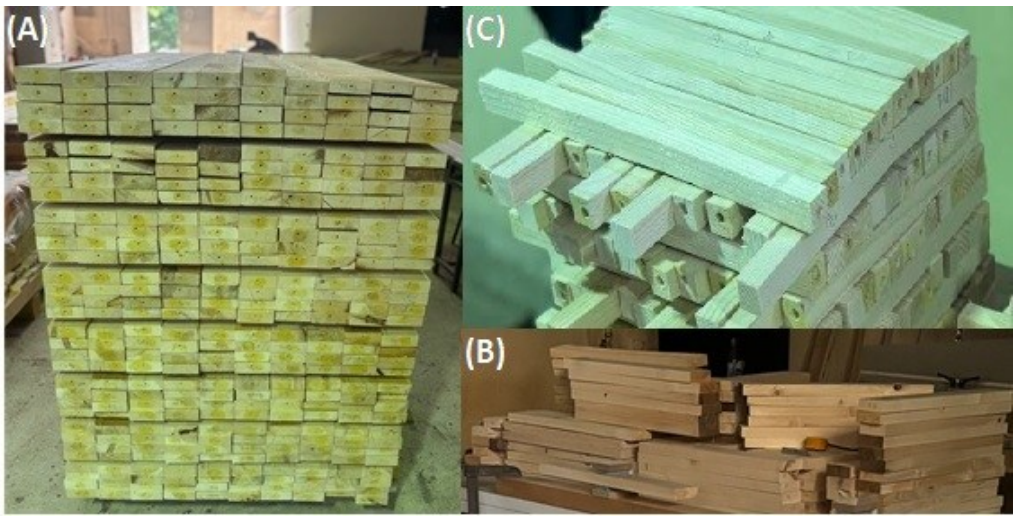

Fig. 2. All test specimens: (A) tension and edgewise bending, (B) flatwise bending, (C) small-clear specimens for 3 and 4-point bending tests

Table 1. Number of Tested Structural Boards for Each Test Type

Species	Group No	Sample Code	Test Type	Dimensions (mm)	Number of Specimens (pcs.)	Moisture Content (%)
Fir	1	A1-A2-B1-B2	Tension and edgewise bending MOE	30 × 90 × 1700	320	13.1
	3	A1-B2	Tension Strength	30 × 90 × 1700	160	13.1
		A2-B1	Edgewise Bending Strength	30 × 90 × 1700	160	13.1
	2,3	C1-C2	Flatwise Bending	30 × 90 × 570	160	13.4
	4	D1-D2-D3	3-Point Bending (Small-Clear)	20 × 20 × 300	122	12.3
		D1-D2-D3	4-Point Bending (Small-Clear)	20 × 20 × 400	122	12.6

Fig. 3. Measuring moisture content using electrical resistance method (Hydrometer HT 65, GANN, Germany)

Visual Grading

From the samples prepared according to Table 1, tensile, edgewise, and flatwise bending samples were visually graded. All defects were measured in accordance with EN 1309-3 (2018b). Visual class limit values for defects were determined according to TS 1265 (2012) as a reference for Class 1, Class 2, Class 3, and Reject (R). Table 2 shows the lower limit values for knot, slope of grain, and rate of growth according to the TS 1265 (2012).

Table 2. Lower Limit Values for Knot, Slope of Grain and Rate of Growth for Each Visual Class According to TS 1265 (2012)

Characteristics	Grades		
	Class 1	Class 2	Class 3
Knot: The ratio of the sum of the narrow, mean, and parallel knot dimensions on each face, to twice the width of the piece (Fig.4).	0.20	0.33	0.50
Slope of grain	Deviation in 1 m length is not greater than:		
a) In case of the presence of surface fissure b) In case of no surface fissure	70 mm 100 mm	120 mm 200 mm	200 mm 300 mm
Annual ring width	The area of annual rings bigger than 4 mm should not exceed 1/2 of the whole cross-sectional area.	No limitation	

Knots were evaluated in three different categories based on knot diameter. These are the narrow knot diameter ratio (NKDR), which refers to the narrow diameter of the knot; the mean knot diameter ratio (MKDR), which refers to the average of the narrow and wide diameters of the knot; and the parallel knot diameter ratio (PKDR), which refers to the diameter parallel to the surface of the knot. Although the limit values in the TS 1265 (2012) are referenced by the PKDR method, the same limit values were used in this study for the other two methods. Knot diameter measurement methods are shown in Fig. 4. The knot diameter ratios for each method are obtained by dividing the reference knot diameters by twice the material width.

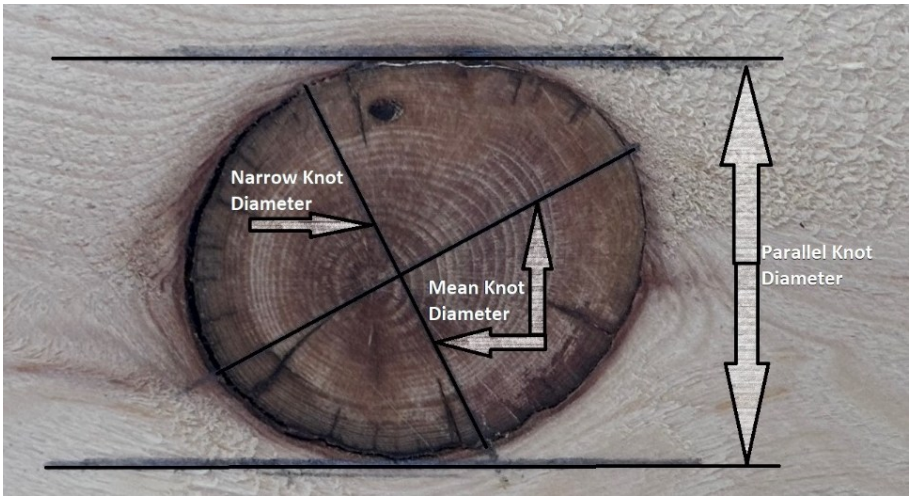

Fig. 4. Knot diameter measuring methods

Non-destructive Tests

After the visual grading, all samples underwent non-destructive testing to determine their dynamic modulus of elasticity. The non-destructive tests used longitudinal vibration-based PLG (Portable Lumber Grader, Fakopp, Hungary) and Hitman HM220 (Fibre-gen, New Zealand) devices. Additionally, a Microsecond Timer (Fakopp, Hungary) based on the time-of-flight (ToF) method, an Ultrasonic Timer (Fakopp, Hungary), and a Sylvatest Duo (Concept Bois Structure, Switzerland) that generates ultrasonic sound waves were used. Additionally, screw withdrawal tests were performed on all samples using a Screw Withdrawal Force Meter (Fakopp, Hungary).

Two dynamic moduli of elasticity based on longitudinal vibration were determined. First, the dynamic modulus of elasticity ($MOEd_{,PLG}$) was calculated for tensile, edgewise, and flatwise bending specimens using the PLG device. The samples were placed on two specially designed supports of the device. A stress wave was generated by striking the end of the board with a hammer. The natural frequency of the material was read using a dynamic microphone and Fast Fourier Transform (FFT) software at the other end of the sample (Fig. 5a). The obtained natural frequency was multiplied by twice the material length to calculate velocity (m/s) for all specimens. Because one of the supports served as a balance, the weight of the specimens was recorded simultaneously. The volume of the specimens was determined by measuring their cross-sectional dimensions, and the density ρ (kg/m^3) was calculated by calculating the ratio of mass to volume. Secondly, the dynamic modulus of elasticity ($MOEd_{,HITMAN}$) was calculated for tensile and edgewise bending specimens using the Hitman HM220 device. The device was pressed against the cross-section of the specimen, and a stress wave was created at the exact location using a hammer (Fig. 5b). The velocity value was read from the device's display and recorded. The dynamic modulus of elasticity based on longitudinal vibration for all specimens was then calculated using Eq. 1,

$$MOE_d = V^2 \times \rho \quad (1)$$

where V (m/s) is the velocity for all test methods, respectively, and ρ (kg/m^3) is the full-size sample's density.

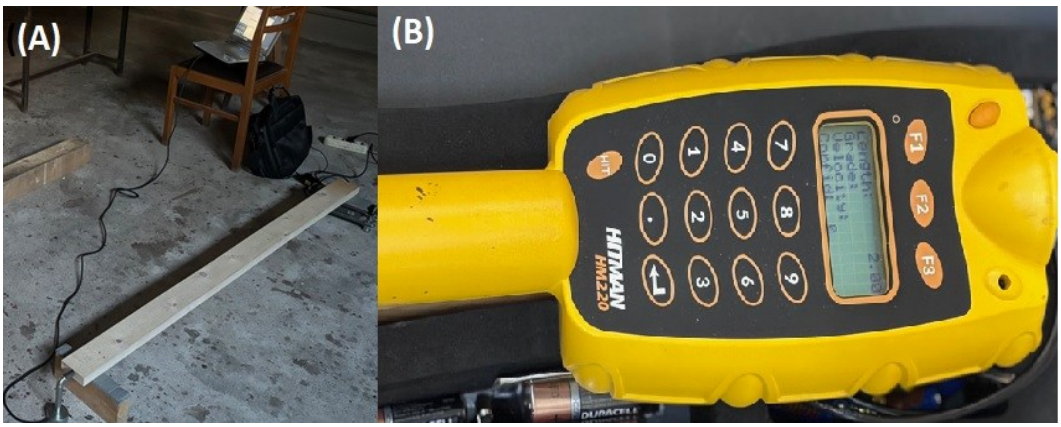

Fig. 5. Longitudinal vibration test setup using PLG (A) and Hitman HM 220 (B) devices

Three dynamic moduli of elasticity based on ToF method were determined. First, the dynamic modulus of elasticity ($MOEd_{,MS}$) was calculated for all samples using a Microsecond Timer device. The device's sensors were placed at both ends of the samples, and the start sensor was struck with a hammer to generate a stress wave. The time required

for this wave to travel the length of the board between the start and the stop sensors was recorded in microseconds (Fig. 6a). The stress wave velocity was determined using the formula distance/time (m/s). Secondly, the dynamic modulus of elasticity ($MOEd_{,UT}$) was calculated for all samples using an Ultrasonic Timer device. The device's sensors were placed at both ends of the samples and secured with wooden wedges. Before each test, ultrasonic gel was applied to the sensors to prevent air gaps from forming between the sensors and the sample. The time required for the generated ultrasonic wave to travel the length of the board between the start and the stop sensors was recorded in microseconds (Fig. 6b). The ultrasonic velocity was determined using the formula m/s. Lastly, the dynamic modulus of elasticity ($MOEd_{,ST}$) was calculated for all samples using the Sylvatest Duo device. First, 5-mm diameter holes were drilled at the center of each board's cross-section. Sensors were placed in these holes, and the time required for the ultrasonic wave to travel the length of the board between the start and stop sensors was recorded in microseconds (Fig. 6c). Ultrasonic velocity was determined using the m/s.

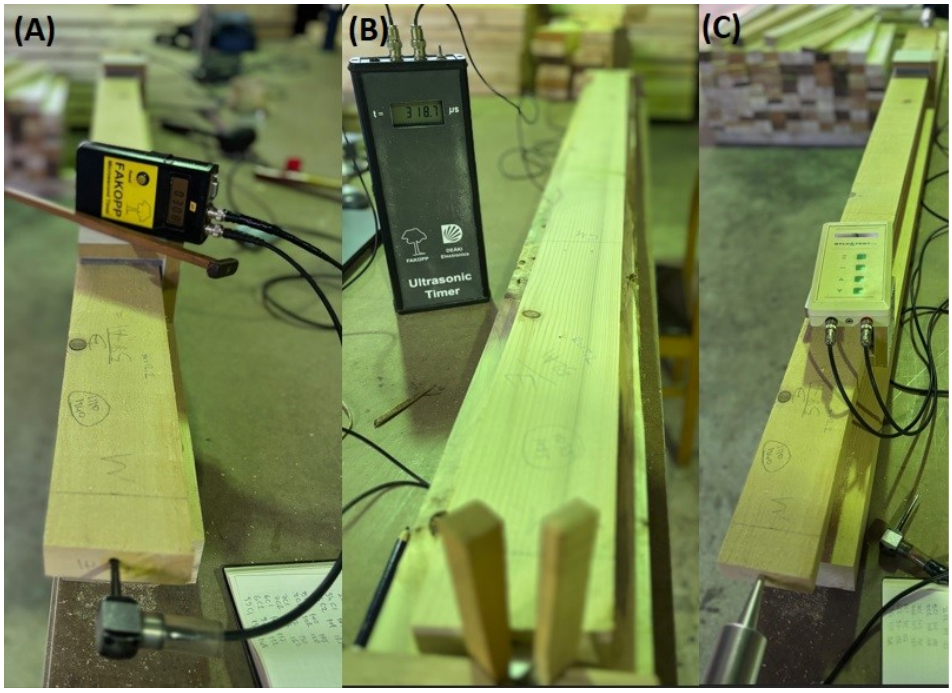

Fig. 6. ToF test setup with Microsecond Timer (A), Ultrasonic Timer (B), and Sylvatest Duo (C)

For all three ToF methods, the dynamic modulus of elasticity was calculated according to Eq. 1. In accordance with EN 14081-2 (2018), the dynamic modulus of elasticity for each method was adjusted to a reference moisture content (MC) of 12%.

The final non-destructive test was the screw withdrawal (SW) test. In this test, 4-mm diameter screws were screwed into all samples to a depth of 18 mm. The device handle was then rotated clockwise at a speed of approximately 0.5 m/s. The maximum load was read and recorded in newton (N) from the device (Fig. 7). For tensile and edgewise bending test samples, measurements were taken from two edges and the average was taken. For flatwise bending and small-clear samples, a single measurement was taken.

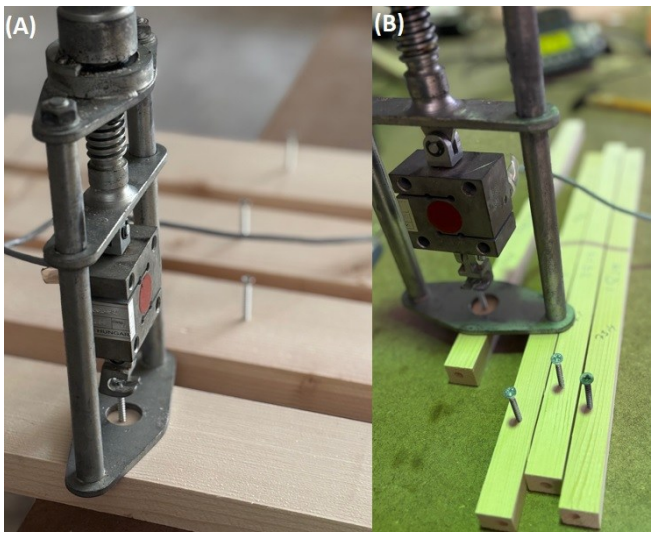

Fig. 7. Screw withdrawal test setup for all boards (A) and small-clear specimens (B)

Mechanical Tests

After non-destructive tests, tensile (MOE_T) and bending modulus of elasticity ($MOE_{B,E}$) tests were conducted on 320 samples coded A1-A2-B1-B2 according to EN 408 (2012). Subsequently, tensile strength (f_T) tests were conducted on 160 samples coded A1-B2 according to the same standard, and edgewise bending strength ($f_{m,E}$) tests were conducted on 160 samples coded A2-B1. Taking the EN 408 (2012) standard as a reference, flatwise bending tests were conducted on 160 samples coded C1-C2, and the modulus of elasticity ($MOE_{B,F}$) and bending strength ($f_{m,F}$) were determined. In addition, the modulus of elasticity ($MOE_{B,C3}$) and bending strength ($f_{M,C3}$) in 3-point bending were determined on 122 small-clear samples according to ISO 13061-3 (2014) and 13061-4 (2014). Additionally, the modulus of elasticity ($MOE_{B,C4}$) and bending strength ($f_{M,C4}$) were determined in 4-point bending on 122 small-clear samples, using EN 408 (2012) as a reference.

Tensile strength and modulus of elasticity in tension parallel to the grain were measured using an 800 kN-capacity horizontal tensile testing machine (BESMAK, Türkiye). The distance between the machine grips was set to 810 mm (9×h), and two LVDTs with 0.001 precision were connected to the gauge at 450 mm (5×h) to measure the deformation (Fig. 8a). In the tensile modulus of elasticity tests, 10000 N was determined as the elastic limit load, and the test speed was adjusted to reach this force within 3 to 5 min.

After determining the tensile modulus of elasticity for all samples, the same sample was subjected to edgewise bending tests to determine the bending modulus of elasticity. Edgewise bending strength and modulus of elasticity in bending tests were performed on a 300 kN capacity bending testing machine (BESMAK, Türkiye). The distance between the supports was set to 1620 mm (18×h), the distance between the loading points to 540 mm (6×h), and the deformation was measured at the midpoint of the sample using a single LVDT with 0.001 precision (Fig. 8b). The elastic limit load for this test was determined as 1200 N. The test speed was adjusted to reach this force within 3 to 5 min. The elastic limit loads for both the tensile and bending modulus of elasticity tests were determined through preliminary tests. The modulus of elasticity in tension parallel to grain and the global modulus of elasticity in edgewise bending were calculated using Eqs. 2 and 3, respectively.

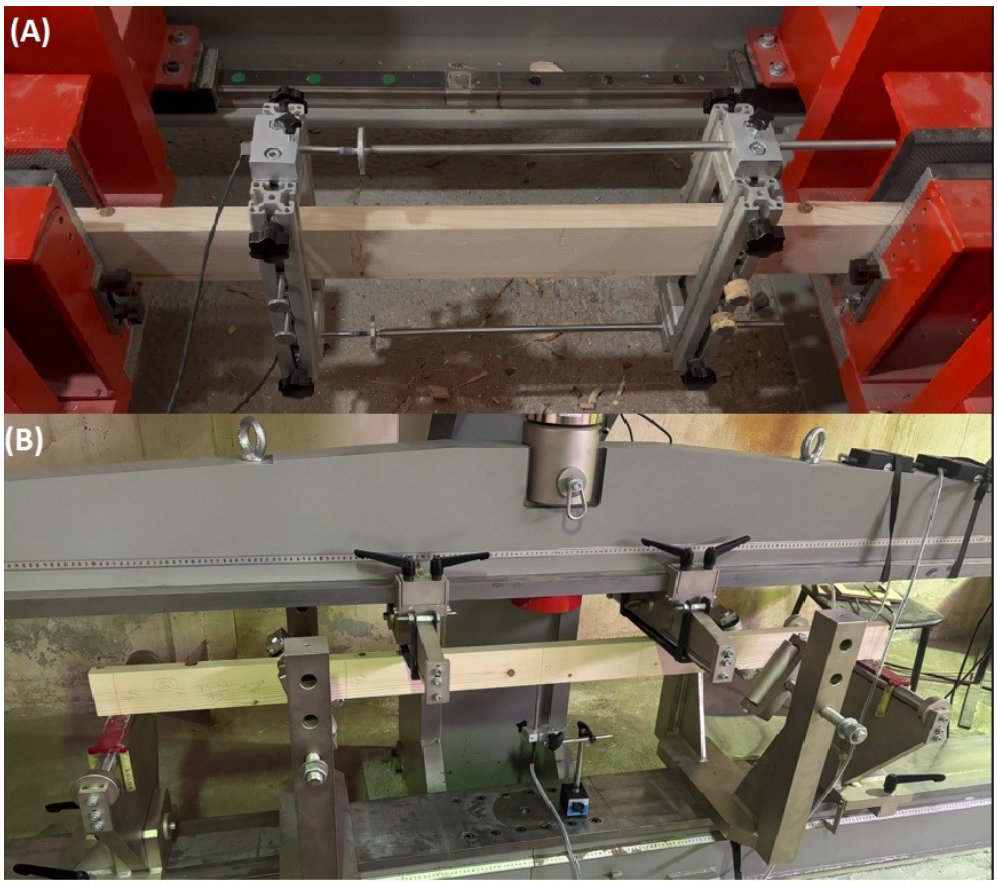

Fig. 8. Test setup for modulus of elasticity in tension parallel to grain (A) and modulus of elasticity in edgewise bending (B) according to EN 408 (2012)

$$MOE_T = \frac{l_1 \times (F_2 - F_1)}{A \times (w_2 - w_1)} \text{ N/mm}^2 \quad (2)$$

$$MOE_{B,E,F,4C} = \frac{3 \times al \times^2 - 4 \times a^3}{2 \times b \times h^3 \times (2 \times \frac{w_2 - w_1}{F_2 - F_1} - \frac{6 \times a}{5 \times G \times b \times h})} \text{ N/mm}^2 \quad (3)$$

In the above equations, MOE_T is the modulus of elasticity in tension parallel to grain (MPa), l_1 is the gauge length (mm), A is the cross-sectional area (mm^2), F_2 - F_1 is the load difference at elastic limit load (N), w_2 - w_1 is the difference between the deformations corresponding to the loads (F_2 and F_1, respectively) at the elastic limit (mm), $MOE_{B,E,F,4C}$ is the modulus of elasticity in bending (for edgewise, flatwise, and 4-point clear samples) (MPa), l is the span distance (mm), a is the distance between a loading point and the nearest support in a bending test (mm), G is the shear modulus assumed as infinitive, b is the width in tension, edgewise and small-clear bending test and height in flatwise test (mm), and h is the height in tension, edgewise, and small-clear bending test and width in flatwise test (mm).

After the modulus of elasticity tests were completed, tensile strength tests (Fig. 9a) were conducted on 160 samples coded A1-B2, and edgewise bending strength tests (Fig. 9b) were conducted on 160 samples coded A2-B1. In both tests, test speed was adjusted to reach maximum load within 3 to 5 min. Tensile strength parallel to the grain was calculated using Eq. 4, and the edgewise bending strength was calculated using Eq. 5.

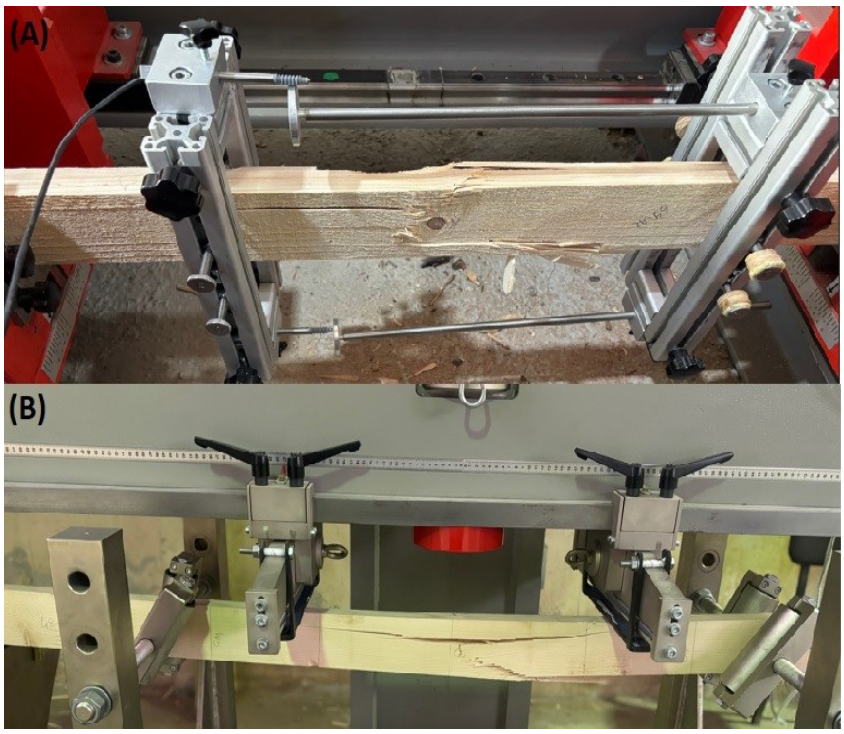

Fig. 9. Tension strength parallel to grain (A) and edgewise bending strength (B)

$$f_T = \frac{F_{max}}{A} \text{ N/mm}^2 \quad (4)$$

$$f_{m,E,F,3C,4C} = \frac{3 \times F_{max} \times a}{b \times h^2} \text{ N/mm}^2 \quad (5)$$

The bending strength for all tests was determined according to Eq. 5 above. Flatwise bending, 3-point bending, and 4-point bending tests were performed on a 10 kN capacity Lloyd LS100 Universal testing machine (METEK, UK). In the flatwise bending tests (Fig. 10a), the distance between the supports was 540 mm (18×h), and the distance between the loading points was 180 mm (6×h).

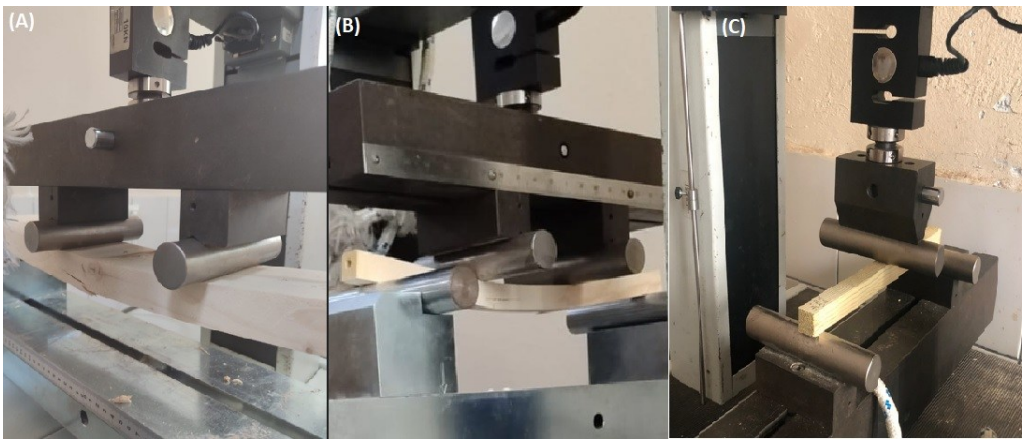

Fig. 10. Flatwise bending (A), 4-point bending (B), and 3-point bending test for clear samples (C)

In the 4-point bending tests on small-clear specimens (Fig. 10b), the distance between the supports was 360 mm (18 h), and the distance between the loading points was 120 mm (6×h). In the 3-point bending tests (Fig. 10c), the distance between the supports

was 280 mm (14×h), and a single loading point was used. Deformation values in the tests were taken from the machine head. The test speed was adjusted to allow the specimens to reach maximum load in 3 to 5 min. The global modulus of elasticity for the flatwise bending and 4-point bending tests on small-clear samples was calculated according to Eq. 3, and the modulus of elasticity for the 3-point bending test was calculated according to Eq. 6.

$$MOE_{B,3C} = \frac{(F_2 - F_1) \times l^3}{4 \times b \times h^3 \times (w_2 - w_1)} \quad \mathrm{N/mm^2} \tag{6}$$

After each mechanical test, the moisture content and density values of the samples were calculated (Fig. 11). To do this, 30 to 40 mm clear sections were cut from the samples near the fracture site after the test. The cut pieces were weighed to the nearest 0.01 g and their dimensions measured to the nearest 0.01 mm. The moisture content of the same samples was also determined according to the procedure described in EN 13183-1 (2002). The test values for all moduli of elasticity and densities of specimens not tested at 12% moisture content were adjusted using the formulas given in EN 384 (2018).

Fig. 11. Moisture content and density samples obtained after mechanical tests

Derivation of Visual Grading Assignments

The method for determining the mechanical property and density characteristic values indicating the strength class for defined visual class populations is given in EN 384 (2018). The strength values for samples with a nominal depth of 90 mm and 30 mm were adjusted to a depth of 150 mm by dividing by the k_h factor, as specified in EN 384 (2018). The global modulus of elasticity was adjusted to the local modulus of elasticity, as specified in the same standard.

After completing the necessary adjustments, the 5th percentile strength values ($f_{0.5}$), defect-free density ($\rho_{0.5}$), and average stiffness values ($E_{0,mean}$) of the fir boards were determined for each knot measurement method and visual class, as specified in EN 14358 (2016). Thus, the impact of changes in KDR ratios on characteristic values and visual classification efficiency was analyzed. Furthermore, the differences between means values were evaluated at a 95% confidence level ($p \leq 0.05$) (IBM SPSS 29.0 software, Armonk, NY, USA) using an independent sample t-test for species comparison and analysis of variance (ANOVA) for all other groups.

RESULTS AND DISCUSSION

The results obtained from visual, non-destructive, and destructive tests are presented separately for each visual grading method and their respective visual classes. The first group includes the average values of the visual, non-destructive, and static modulus of elasticity tests performed on samples coded A1-B2-A2-B1 (Table 3), the second group includes the average values of the visual, non-destructive, and static modulus of elasticity tests performed on samples coded C1-C2 (Table 4), and the third group includes the average strength values for the first three groups are presented separately for the visual grading method and its respective visual classes (Table 5). In the final group, includes the average values non-destructive and destructive tests performed on samples coded D1-D2-D3 (Table 7). In addition, the relationships between tensile, edgewise and flatwise bending tests, non-destructive tests, and knot diameter measurement methods are given in Table 6. The relationships between 3- and 4-point bending tests on small-clear specimens and non-destructive tests are given in Table 8. The average values of non-destructive and destructive tests were adjusted to a 12% M.C.

According to Tables 3 and 4, the average extent of growth for the tested samples was 2.96 mm. Because the TS 1265 (2012) standard classifies samples with growth greater than 4 mm as Class 2, the average growth of Class 1 samples was lower than that of the other groups across all three visual grading methods. The average knot diameter ratios remained within the class limit values given in the same standard. Only Class 2 samples in the NKDR group failed to comply with this condition for flatwise bending tests. The effect of growth was decisive in this group. It was determined that the knot diameter ratios in the flatwise bending test samples were lower in all groups compared to the tensile and edgewise bending test samples. The average moisture content of the samples was 12.6%, and the average air-dry density was 388 kg/m^3. Kurul and associates (Kurul *et al.* 2024; Kurul 2025; Kurul *et al.* 2025) determined the air-dry density values for the fir species as 410, 412, and 417 kg/m^3 in their studies.

Table 3 shows that the average dynamic modulus of elasticity was 9,209 MPa and 8,804 MPa for the Hitman and PLG devices, respectively, measured by the vibration method. The PLG gave a dynamic modulus of elasticity value approximately 4.6% higher than the Hitman. The average dynamic modulus of elasticity was calculated as 10,956 MPa for the MT, 10,428 MPa for the UT, and 12,264 MPa for the ST, measured by the ToF method. The measurement ratios between the devices were determined as 1, 0.95, and 1.12, respectively. When the vibration method and ToF methods were compared, it was determined that the PLG device was 19%, 13%, and 33% lower, respectively, and the Hitman device was 24%, 18%, and 39% lower, respectively, than the ToF-based devices. Table 4 shows that the average dynamic modulus of elasticity for flatwise bending samples was 8,825 MPa for the PLG device. Due to the length of the samples, measurements could not be made with the Hitman. In devices measuring using the ToF method, the average dynamic modulus of elasticity was calculated as 9,887 MPa, 10,132 MPa, and 14,217 MPa, respectively. The measurement ratios between the devices were determined as 1, 1.03, and 1.44, respectively. Compared to the PLG measurement, 12%, 15%, and 61% higher values were obtained, respectively. It was found that as the sample length decreased, the values read from the ST increased, and the measurement ratio between the devices increased.

Table 3. Descriptive Statistics of the Measured Visual, Non-destructive and Static Elastic Properties for Samples coded A1-B2 and A2-B1 (Group 1)

Visual Grading Methods													
Method	Narrow Knot Diameter Ratio (NKDR)				Mean Knot Diameter Ratio (MKDR)				Parallel Knot Diameter Ratio (PKDR)				Total
Class	1	2	3	R	1	2	3	R	1	2	3	R	
Number of samples	134	133	47	6	85	125	88	22	81	131	81	27	320
Rate of Growth (mm)	2.70 (22.0)	3.24 (33.2)	2.88 (30.0)	3.81 (19.5)	2.69 (22.1)	3.00 (32.5)	3.14 (32.3)	3.24 (23.9)	2.7 (22.3)	2.98 (33.0)	3.11 (31.2)	3.36 (25.9)	2.97 (30.4)
KDR	0.126 (45.7)	0.241 (25.0)	0.378 (12.7)	0.541 (4.1)	0.122 (48.3)	0.245 (22.0)	0.406 (11.4)	0.595 (13.9)	0.123 (49.4)	0.242 (21.8)	0.393 (12.2)	0.563 (17.4)	0.281 (52.1)
M.C. (%)	12.4 (7.6)	12.4 (7.8)	12.3 (7.2)	12.0 (6.2)	12.3 (8.0)	12.3 (7.5)	12.5 (7.3)	12.4 (7.5)	12.3 (8.1)	12.4 (7.4)	12.5 (7.1)	12.4 (8.3)	12.4 (7.6)
ρ (kg/m^3)	399 (7.7)	380 (7.2)	382 (7.0)	395 (6.3)	404 (7.9)	384 (7.1)	380 (7.0)	391 (6.5)	402 (8.2)	386 (7.1)	382 (7.7)	382 (5.7)	389 (7.4)
MOEd,$_{PLG}$ (MPa)	10,166 (15.9)	8,818 (16.2)	7,934 (17.6)	6,483 (12.9)	10,447 (15.9)	9,453 (14.3)	7,557 (19.9)	7,553 (18.7)	10,353 (16.0)	9,533 (14.7)	8,135 (16.6)	7,423 (19.8)	9,209 (19.0)
MOEd,$_{HITMAN}$ (MPa)	9,745 (15.4)	8,414 (15.8)	7,542 (15.6)	6,360 (12.0)	10,026 (15.3)	9,028 (14.1)	7,888 (16.2)	7,165 (15.5)	9,924 (15.4)	9,104 (14.5)	7,730 (15.4)	7,216 (18.5)	8,804 (18.5)
MOEd,$_{MT}$ (MPa)	11,607 (11.4)	10,611 (11.4)	10,302 (12.4)	9,190 (9.3)	11,755 (11.8)	11,006 (10.8)	10,336 (12.4)	10,058 (12.5)	11,730 (11.7)	11,063 (10.9)	10,324 (12.3)	10,089 (13.7)	10,956 (12.7)
MOEd,$_{UT}$ (MPa)	11,154 (14.7)	10,053 (14.5)	9,708 (15.0)	8,132 (5.2)	11,349 (14.7)	10,529 (13.3)	9,686 (15.9)	9,262 (15.0)	11,299 (14.4)	10,602 (13.5)	9,691 (15.7)	9,180 (16,7)	10,428 (15.9)
MOEd,$_{ST}$ (MPa)	12,995 (12.0)	11,853 (12.5)	11,581 (13.1)	10,396 (8.6)	13,132 (12.7)	12,326 (11.2)	11,575 (13.7)	11,312 (13.2)	13,091 (12.3)	12,384 (11.6)	11,572 (13.6)	11,275 (14.3)	12,264 (13.4)
SW (N)	1,194 (15.9)	1,103 (14.3)	1,103 (14.2)	1,218 (10.0)	1,204 (16.2)	1,116 (14.9)	1,131 (15.1)	1,117 (12.0)	1,192 (16.7)	1,130 (14.0)	1,121 (16.6)	1,135 (12.3)	1,144 (15.4)
MOE$_T$ (MPa)	9,482 (16.7)	8,155 (18.3)	6,972 (22.0)	5,764 (20.9)	9,762 (16.2)	8,814 (15.5)	7,292 (20.3)	6,561 (23.6)	9,666 (16.7)	8,871 (15.8)	7,283 (20.4)	6,762 (24.5)	8,492 (21.3)
MOE$_{B,E}$ (MPa)	8,963 (16.1)	7,732 (16.3)	6,652 (18.2)	5,096 (20.6)	9,240 (15.5)	8,294 (14.8)	6,991 (17.2)	6,146 (20.8)	9,135 (15.4)	8,359 (15.3)	6,948 (18.4)	6,469 (21.8)	8,039 (20.0)

(Values in parentheses represent coefficients of variation, %)

Table 4. Descriptive Statistics of the Measured Visual, Non-destructive and Static Elastic Properties for Samples Coded C1-C2 (Group 2)

Visual Grading Methods													
Method	Narrow Knot Diameter Ratio (NKDR)				Mean Knot Diameter Ratio (MKDR)				Parallel Knot Diameter Ratio (PKDR)				Total
Class	1	2	3	R	1	2	3	R	1	2	3	R	
Number of samples	93	51	16	-	76	56	24	4	79	48	30	3	160
Rate of Growth (mm)	2.71 (22.5)	3.34 (30.8)	2.99 (38.5)	-	2.70 (22.6)	3.26 (31.0)	3.01 (33.6)	2.33 (12.0)	2.68 (22.8)	3.16 (32.3)	3.29 (30.7)	2.54 (9.8)	2.94 (29.6)
KDR	0.064 (60.3)	0.195 (49.2)	0.268 (58.6)	-	0.054 (65.3)	0.211 (42.2)	0.338 (41.1)	0.531 (2.7)	0.055 (68.5)	0.208 (44.2)	0.351 (36.6)	0.548 (22.9)	0.163 (71.4)
M.C. (%)	13.0 (4.0)	12.9 (3.1)	13.0 (2.6)	-	12.9 (4.1)	13.0 (3.3)	13.0 (2.6)	13.0 (3.8)	12.9 (4.1)	13.0 (3.2)	13.0 (2.8)	12.9 (1.6)	13.0 (3.6)
ρ (kg/m^3)	388 (8.1)	384 (6.9)	376 (6.3)	-	388 (8.3)	386 (7.2)	385 (6.2)	353 (1.6)	388 (8.0)	387 (7.1)	382 (7.4)	363 (5.3)	386 (7.6)
MOEd,$_{PLG}$ (MPa)	9,347 (18.1)	8,393 (15.1)	7,064 (21.9)	-	9,388 (17.5)	8,682 (17.6)	7,490 (19.5)	7,934 (26.7)	9,356 (17.4)	8,976 (15.5)	7,326 (19.8)	6,741 (18.5)	8,825 (19.3)
MOEd,$_{MT}$ (MPa)	10,085 (11.8)	9,767 (11.3)	9,065 (12.7)	-	10,054 (13.5)	9,956 (13.1)	9,271 (11.5)	9,275 (13.3)	10,077 (13.1)	10,133 (12.1)	9,050 (12.3)	9,028 (14.9)	9,887 (13.3)
MOEd,$_{UT}$ (MPa)	10,337 (13.7)	9,935 (10.9)	9,526 (12.0)	-	10,354 (12.8)	10,061 (13.7)	9,648 (10.8)	9,695 (7.9)	10,372 (12.6)	10,217 (12.8)	9,409 (12.1)	9,421 (9.1)	10,132 (13.0)
MOEd,$_{ST}$ (MPa)	14,513 (12.1)	13,910 (13.5)	13,429 (13.6)	-	14,479 (11.6)	14,043 (15.0)	13,791 (12.0)	14,239 (6.8)	14,494 (11.3)	14,249 (15.1)	13,465 (12.1)	13,776 (4.6)	14,217 (12.9)
SW (N)	1,126 (20.6)	1,158 (19,9)	1,092 (19.1)	-	1,127 (20.7)	1,144 (16,6)	1,145 (16,7)	987 (6.9)	1,125 (20.6)	1,145 (19.2)	1,139 (19.3)	1,108 (24.5)	1,133 (20.0)
MOE$_{B,F}$ (MPa)	8,876 (13.2)	7,769 (17.8)	6,611 (22.3)	-	8,925 (12.1)	8,166 (16.3)	6,819 (23.8)	7,222 (30.9)	8,910 (11.9)	8,396 (15.2)	6,760 (21.1)	5,606 (2.4)	8,307 (17,6)

(Values in parentheses represent coefficients of variation, %)

In similar studies in the literature, the vibration method was reported to be approximately 16% lower than the ToF method by Kurul (2025) and Kurul and As (2024), and approximately 14% lower by Montero *et al.* (2015). This is because, in the TOF method, the generated stress wave is less affected by defects as it travels the shortest distance between the two sensors, whereas in the vibration method, it is more affected by defects as it scans the entire wood volume (Kurul and As 2024).

According to Tables 3 and 4, the screw withdrawal forces for the samples were 1,144 N and 1,133 N, respectively. The average values of the modulus of elasticity in tensile, edgewise bending, and flatwise bending were determined as 8,492, 8,039, and 8,307 MPa, respectively. The ratios between the tests were calculated as 1, 0.95, and 0.98, respectively. A higher modulus of elasticity was determined in flatwise bending tests than in edgewise bending tests. Similarly, Kurul (2025) reported that a higher global modulus of elasticity was obtained in flatwise bending tests. However, when explicitly examined in terms of visual classes, it was observed that edgewise tests yielded higher elastic modulus values than flatwise tests. Higher values of tensile modulus were obtained than in both the bending test methods. An ANOVA was performed to determine whether the knot diameter measurement methods differed statistically in their estimates of modulus of elasticity. Then, the Duncan test was performed to determine which group or groups showed significant differences from each other. The lowercase letters above the values in Fig. 12 indicate the difference between the visual grading methods for each test. According to the results, the NKDR measurement method differed from the other methods only for Class 2 boards. This is thought to be due to the growth effect in Class 2 samples. Therefore, it can be concluded that the knot diameter measurement methods did not cause a significant difference in the average modulus of elasticity values for the three test types.

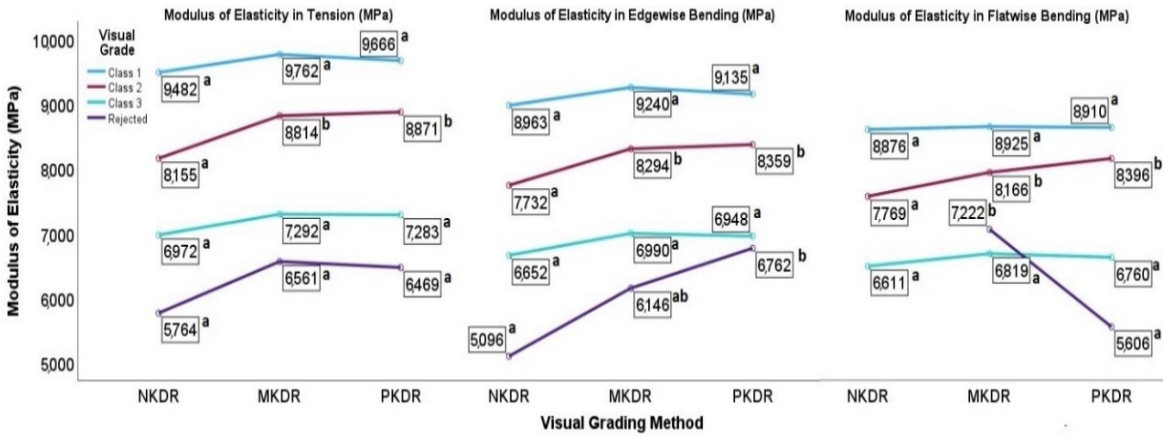

Fig. 12. ANOVA result for each stiffness test according to visual grading method

Table 5 presents the average tensile strength, edgewise bending strength, and flatwise bending strength for visual classes for each visual grading method. Flatwise bending strength was found to be approximately 16% higher than edgewise bending strength and approximately 31% higher than tensile strength for Class 1 for all visual grading methods. It was found to be approximately 27% to 65% and 31% to 76% higher for Class 2 and Class 3, respectively. Comparing edgewise bending strength with tensile strength, it was determined that the values were approximately 11%, 38%, and 45% higher for Class 1, Class 2, and Class 3, respectively. As visual class deteriorates, the difference between tensile and bending strengths increases. It can be said that tensile strength is more

affected by defects than bending strength. Higher bending strength values were calculated in flatwise bending compared to edgewise bending. This may be because the effect of the height (h) value in the denominator of the bending strength formula is greater than the effect of the maximum force (F_{max}) obtained (Kurul 2025). Furthermore, the lower knot ratios in the flatwise samples also affected this situation.

Table 5. Descriptive Statistics of the Destructive Tests for Samples Coded A1-B2, A2-B1, and C1-C2 (Group 3)

Visual Grading Methods												
Method	Narrow Knot Diameter Ratio (NKDR)				Mean Knot Diameter Ratio (MKDR)				Parallel Knot Diameter Ratio (PKDR)			
Class	1	2	3	R	1	2	3	R	1	2	3	R
Number of samples	65	71	22	2	39	63	49	9	38	68	41	13
f_T (MPa)	35.7 (32.2)	22.9 (37.0)	18.8 (23.7)	8.5 (7.5)	38.9 (28.3)	28.1 (33.0)	19.6 (35.1)	14.7 (38.0)	38.6 (29.4)	27.9 (32.3)	19.3 (36.8)	17.4 (55.0)
Number of samples	69	62	25	4	46	62	39	13	43	63	40	14
$f_{m,E}$ (MPa)	40.9 (22.3)	33.5 (26.6)	27.4 (30.4)	17.3 (50.4)	42.7 (18.2)	36.8 (23.9)	27.9 (29.7)	24.8 (41.5)	42.2 (19.2)	37.9 (23.2)	28.2 (30.2)	23.2 (32.3)
Number of samples	93	51	16	-	76	56	24	4	79	48	30	3
$f_{m,F}$ (MPa)	48.9 (16.0)	41.3 (20.3)	31.5 (25.6)	-	49.7 (15.3)	43.6 (17.4)	33.4 (25.7)	34.8 (36.7)	49.5 (15.3)	44.7 (15.9)	33.8 (23.8)	26.2 (16.8)

(Values in parentheses represent coefficients of variation, %)

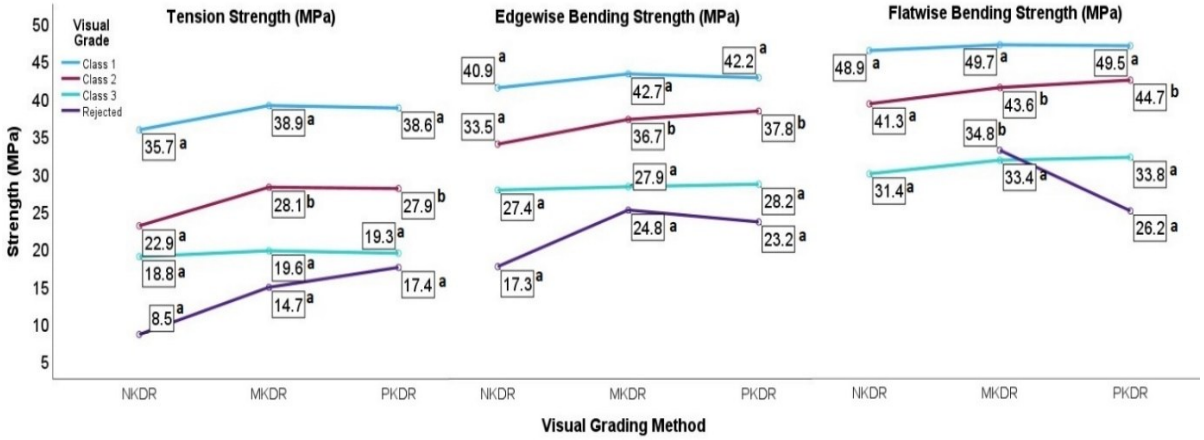

Fig. 13. ANOVA result for each strength test according to visual grading method

An ANOVA was conducted to determine whether the visual grading methods differed statistically during the strength tests. Then the Duncan test was conducted to determine which groups caused the differences. The lowercase letters above the values in Fig. 13 indicate the difference between the visual classification methods for each test. The results obtained were similar to those for the modulus of elasticity. Therefore, it can be concluded that differences in the visual classification methods did not result in a significant difference in average strength values.

A Pearson correlation matrix was created to show the relationships between static tests, non-destructive tests, and visual grading methods (Table 6). In Table 6, bold numbers indicate strong correlations, underlined number indicate moderate correlations, and italic number indicate weak correlations.

Table 6. Correlation Matrix for Destructive Tests, Non-destructive Tests, and Visual Grading Methods in Group 1, 2, and 3 Tests

R	Static Tests				Non-destructive Tests						Visual Grading Methods		
	MOE_T	f_T	$MOE_{B(E,F)}$*	$f_{m,(E,F)}$*	$MOEd_{,PLG}$	$MOEd_{,HITMAN}$	$MOEd_{,MT}$	$MOEd_{,UT}$	$MOEd_{,ST}$	SW	NKDR	MKDR	PKDR
MOE_T	**1**	**0.817**	**0.917**	**0.711**	**0.922**	**0.927**	**0.822**	**0.843**	**0.785**	*0.197*	0.497	0.518	0.504
f_T	**0.817**	**1**	**0.751**	-	**0.792**	**0.803**	0.656	0.667	0.621	*0.201*	0.597	0.626	0.626
$MOE_{B,E}$	**0.917**	**0.751**	**1**	**0.759**	**0.929**	**0.934**	**0.854**	**0.856**	**0.810**	*0.219*	0.532	0.558	0.524
$f_{m,E}$	**0.711**	-	**0.759**	**1**	0.659	0.682	0.579	0.566	0.557	*0.185*	0.524	0.566	0.543
$MOE_{B,F}$	-	-	**1**	**0.831**	**0.839**	-	0.693	0.699	0.695	*0.060*	0.301	0.369	0.413
$f_{m,F}$	-	-	**0.831**	**1**	**0.723**	-	0.518	0.536	0.533	*0.179*	0.437	0.484	0.508

Among the visual classification methods, MKDR and PKDR showed similar correlations and were higher than NKDR. In non-destructive measurements, the two devices used in the vibration method produced similar results, with the Hitman device slightly ahead. Although the same pattern was observed in all three devices used in the ToF method, the Ultrasonic Timer device was seen to be one step ahead. The vibration method was found to be more successful in predicting material quality than the ToF method and to have higher correlations. Kurul and As (2024), Arriaga *et al.* (2012), Gil-Moreno *et al.* (2022), and Nocetti *et al.* (2010) also reported a stronger correlation with the vibration method than with the ToF method. When examining the static tests, very high correlations were found between tensile and edgewise bending tests. The relationships between strength values and knot ratios, in particular, indicate that knot ratios should be considered as a variable in machine strength classification. Screw withdrawal shows a weak correlation with strength and elasticity. Because the test is applied at a local point and the samples contain defects, it is believed that it alone cannot provide a reliable estimate of material strength.

Table 7. Descriptive Statistics of the Non-destructive and Destructive Tests for Samples Coded D1-D2-D3 (Group 4)

Method	3-Point Bending	4-Point Bending	Total
Number of samples	122	122	244
MC (%)	11.7 (5.0)[a]	12.1 (6.0)[a]	11.9 (5.8)
ρ (kg/m^3)	401 (8.4)[a]	399 (9.2)[a]	400 (8.8)
$MOEd_{,MT}$ (MPa)	9,103 (13.1)[a]	9,169 (13.0)[a]	9,136 (13.0)
$MOEd_{,UT}$ (MPa)	9,855 (15.3)[a]	9,762 (14.9)[a]	9,809 (15.1)
$MOEd_{,ST}$ (MPa)	15,133 (15.2)[a]	15,091 (15.3)[a]	15,112 (15.2)
SW (N)	1,363 (16.9)[a]	1,370 (18.4)[a]	1,367 (17.6)
$MOE_{B,C}$ (MPa)	6,759 (16.2)[a]	8,349 (15.5)[b]	-
$f_{m,C}$ (MPa)	47.7 (15.5)[a]	53.3 (14.8)[b]	-

Table 7 shows the destructive and non-destructive test results for 3- and 4-point bending tests on small-clear samples. A t-test was conducted to determine whether there was a statistically significant difference between the three-point and four-point bending tests. Lowercase letters above the mean values in the table indicate differences between groups. For defect-free samples, the average dynamic modulus of elasticity was calculated

as 9,136 MPa for the MT, 9,809 MPa for the UT, and 15,112 MPa for the ST, all using the ToF method. The measurement ratios between the devices were determined to be 1, 1.07, and 1.65, respectively. Although the results were similar to those obtained for the sample which has a defect, the values obtained with the ST device were even higher. The screw withdrawal force was 1,367 N. Because defect-free surfaces were used for the tests on defective samples, the results were similar. The average values of the modulus of elasticity in 3- and 4-point bending were determined as 6,759 MPa and 8,349 MPa, respectively. Due to the lower support span (14 h) in the 3-point bending test, the 4-point test yielded a 23% higher value. Kurul *et al.* (2025) reported a 31% difference in their study. In 4-point bending, similar values were obtained for the modulus of elasticity of flatwise bending tests in Class 1. When the average modulus of elasticity values in 3- and 4-point bending were compared, it was seen that the modulus values obtained in 4-point tests were higher. Fatih *et al.* (2025) found similar results in their study. The average bending strength was 47.7 and 53.3 MPa for the 3-point and 4-point tests, respectively. Although Kurul *et al.* (2025) found the values obtained from the 4-point tests to be higher in their study, they did not detect a statistically significant difference. The difference found in this study was statistically significant. When compared with flatwise and edgewise bending strength in Class 1, defect-free samples exhibited higher bending strength, as expected. Table 8 shows the correlations between the 3- and 4-point bending tests performed on defect-free samples and with non-destructive tests. Among the non-destructive devices, UT showed the highest correlation with the other devices. In the screw withdrawal tests, moderate correlations were found with the strength properties after the influence of defects was eliminated. Strong correlations were found for the strength and stiffness properties, as in the other test groups.

Table 8. Correlation Matrix for Destructive and Non-destructive Tests in Group 4

R	Static Tests		Non-destructive Tests			
	MOE_{BC}	$f_{m,C}$	$MOEd_{,MT}$	$MOEd_{,UT}$	$MOEd_{,ST}$	SW
$MOE_{B,C3}$	**1**	**0.852**	**0.771**	**0.813**	**0.783**	*0.298*
$f_{m,C3}$	**0.852**	**1**	0.521	0.590	0.512	0.513
$MOE_{B,C4}$	**1**	**0.736**	**0.766**	**0.860**	**0.850**	*0.149*
$f_{m,C4}$	**0.736**	**1**	0.532	0.669	0.652	0.335

Figure 14 shows that an ANOVA test was conducted to examine whether the average dynamic modulus of elasticity values obtained from the non-destructive devices used for each test group differed. Lowercase letters in parentheses indicate differences in Group 1, lowercase letters in parentheses indicate differences in Group 2, and lowercase numbers indicate differences in Group 4. Accordingly, it was determined that the test devices used for each group differed statistically. While the PLG, MS, and US devices yielded lower dynamic modulus of elasticity as the sample length decreased, the ST device, conversely, yielded higher values. The use of the Hitman and PLG devices was restricted as sample lengths decreased.

Table 9 shows the characteristic values for each visual class for the three visual grading methods, determined separately for the tensile (T), edgewise, and flatwise bending (C) tests according to EN 338 (2020). Bending strength classes are given in parentheses next to the tensile strength classes, and tensile strength classes are given in parentheses next to the bending strength classes, in reference to EN 14080 (2013). While the MKDR and PKDR methods exhibited similar tension strength properties, the NKDR method showed lower-strength classes. For all visual grading methods, density was the determining

characteristic for Class 1 boards, modulus of elasticity for Class 2 boards, and tensile strength for Class 3 boards.

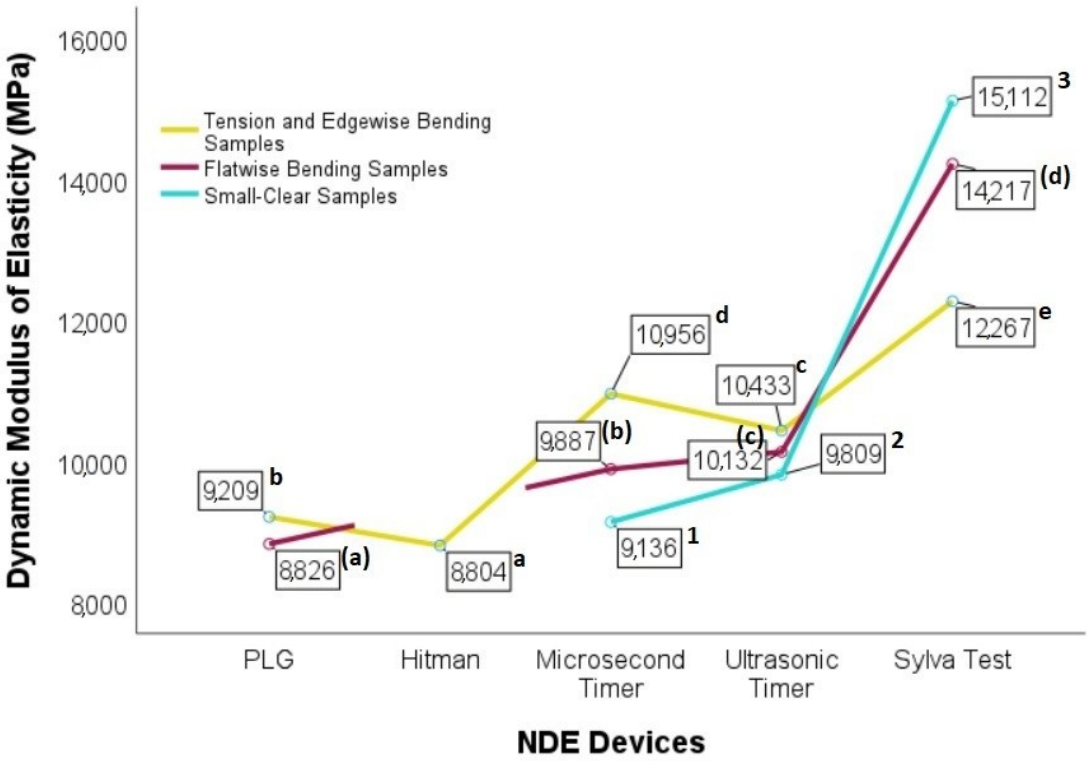

Fig. 14. Moisture content and density samples obtained after mechanical tests

The bending strength classes calculated from edgewise bending tests showed similar properties in the MKDR and PKDR methods, such as tensile tests. Lower-strength classes were obtained using the NKDR method. Class 3 boards were not assigned to any strength class. The modulus of elasticity was the grade-determining property in all visual classes. The same strength classes were calculated for all methods as a result of the flatwise bending tests. The modulus of elasticity was the grade-determining property, like in the edgewise test. Because lower modulus values were calculated in flatwise tests compared to edgewise tests for Class 1, the strength classes for Class 1 boards were also lower. Class 2 boards were assigned to similar strength classes. Class 3 boards, however, were not assigned to a strength class as in the edgewise tests.

A comparison of all tests revealed that similar strength classes were obtained using three different visual grading methods. Because the modulus of elasticity was determined locally, it is thought that the resulting strength classes will be similar. Kurul and As (2024) reported in their study that local modulus of elasticity tests yielded values approximately 15% higher than those of global modulus of elasticity tests. Furthermore, when the conversion from global to local modulus of elasticity is applied according to the EN 384 (2018) standard, samples with modulus of elasticity values lower than 9,000 MPa result in lower modulus of elasticity values (Kurul 2025). This resulted in lower modulus of elasticity values in Class 2 and Class 3 samples. Consequently, differences in strength classes were observed.

Table 9. The Characteristic Values for Each Visual Class According to all Visual Grading and Test Methods.

Test Type	Visual Grading Methods	Visual Grade	f_{mean} (MPa)	$f_{0.5}$ (MPa)	Strength Class	$E_{0,mean}$ (MPa)	Strength Class	ρ_{mean} (kg/m^3)	$\rho_{0.5}$	Strength Class	Result
Tension Strength (f_t)	Narrow Knot Diameter Ratio	1	32.2	16.2	T16(C27)	10,112	T13(C22)	397	331	T12(C20)	T12(C20)
		2	20.5	9.3	T9(C14)	8,672	T10(C16)	378	331	T12(C20)	T9(C14)
		3	17.0	10.1	T10(C16)	7,802	T9(C14)	381	329	T11(C18)	T9(C14)
	Mean Knot Diameter Ratio	1	35.2	19.6	T18(C30)	10,455	T13(C22)	407	335	T12(C20)	T12(C20)
		2	25.1	12.2	T12(C20)	9,380	T11(C18)	377	335	T12(C20)	T11(C18)
		3	17.7	8.8	T8(C14)	8,005	T10(C16)	379	327	T11(C18)	T8(C14)
	Parallel Knot Diameter Ratio	1	34.9	18.7	T18(C30)	10,242	T13(C22)	403	333	T12(C20)	T12(C20)
		2	24.9	12.4	T12(C20)	9,409	T11(C18)	380	337	T12(C20)	T11(C18)
		3	17.4	8.6	T8(C14)	8,044	T10(C16)	383	326	T11(C18)	T8(C14)
Edgewise Bending Strength (f_m)	Narrow Knot Diameter Ratio	1	36.9	22.7	C22(T13)	9,374	C18(T11)	401	357	C18(T11)	C18(T11)
		2	30.2	17.6	C16(T10)	7,852	C14(T8)	384	333	C14(T8)	C14(T8)
		3	24.7	12.7	-	5,840	-	383	333	-	-
	Mean Knot Diameter Ratio	1	38.6	26.5	C24(T14)	9,667	C20(T12)	402	356	C24(T14)	C20(T12)
		2	33.2	19.9	C18(T11)	8,603	C16(T10)	390	338	C20(T12)	C16(T10)
		3	25.2	14.4	C14(T8)	6,428	-	381	337	C20(T12)	-
	Parallel Knot Diameter Ratio	1	38.1	25.7	C24(T14)	9,534	C20(T12)	401	359	C24(T14)	C20(T12)
		2	34.2	20.5	C20(T12)	8,761	C16(T10)	392	339	C20(T12)	C16(T10)
		3	25.5	13.9	-	6,427	-	381	330	C18(T11)	-
Flatwise Bending Strength (f_m)	Narrow Knot Diameter Ratio	1	37.6	27.6	C27(T16)	9,315	C18(T11)	388	332	C20(T12)	C18(T11)
		2	31.8	20.9	C20(T12)	7,800	C14(T8)	384	336	C20(T12)	C14(T8)
		3	24.2	12.9	-	6,215	-	377	330	C20(T12)	-
	Mean Knot Diameter Ratio	1	38.2	28.5	C27(T16)	9,381	C18(T11)	388	330	C20(T12)	C18(T11)
		2	33.6	23.9	C22(T13)	8,343	C16(T10)	386	336	C20(T12)	C16(T10)
		3	25.7	14.2	C14(T8)	6,500	-	386	341	C22(T13)	-
	Parallel Knot Diameter Ratio	1	38.1	28.5	C27(T16)	9,361	C18(T11)	388	332	C20(T12)	C18(T11)
		2	34.4	25.2	C24(T14)	8,658	C16(T10)	397	336	C20(T12)	C16(T10)
		3	26.0	15.2	C14(T8)	6,419	-	382	330	C20(T12)	-

CONCLUSIONS

1. While there were no significant differences in the average strength and modulus of elasticity across all tests based on visual grading methods, significant differences were found in the characteristic strength values. The MKDR and PKDR methods yielded higher correlations with destructive and non-destructive tests than the NKDR method. Furthermore, these two methods achieved higher tensile and bending strength classes. Because the MKDR and PKDR methods yield similar results, they are considered interchangeable. The EN 1309-3 (2018) standard recommends the MKDR method and emphasizes the PKDR method as an alternative. In practice, the PKDR method is considered a step ahead because it offers easier, faster measurement opportunities.
2. According to non-destructive test results, a difference of approximately 5% was found between the PLG and Hitman devices, which are based on the vibration method. The Hitman device stood out for its stronger correlation with destructive tests. Moderate correlations were observed between the MT, UT, and ST devices and destructive tests. When all correlations were examined, the UT was found to be the leading device. However, because the UT and ST methods require preprocessing during application, the MT is considered more advantageous in practice. It was determined that the MOEd obtained with the ToF method was generally higher than the MOEd obtained with the vibration method. Furthermore, the vibration method showed higher correlations with destructive tests than the ToF method. Therefore, it proved more successful in determining wood quality. However, the ToF method may be preferred for short sample lengths and for *in-situ* applications (*e.g.*, evaluating structural elements in a wooden building or bridge). It is thought that screw withdrawal tests alone are not sufficient to understand material quality and can be used in integration with other non-destructive methods.
3. According to the destructive test results, the highest strength values were found in flatwise bending, edgewise bending, and tensile tests, respectively. The order of elastic modulus values was the opposite. Tensile strength was found to be more affected by defects than bending strength. Furthermore, there was a significant decrease in strength as the knot diameter ratio increased. When adjustment from global to local modulus of elasticity, lower values were obtained for modulus of elasticity below 9,000 MPa. Therefore, Class 2 and Class 3 materials were assigned to lower strength classes despite having high strength values. It is believed that higher strength classes can be achieved for visual and machine strength grading by opting for local tests.
4. Tensile and bending characteristic values were calculated for three different visual grading methods and for each visual class. For all methods, it was determined that as the visual class deteriorates, the strength classes decrease. Although tensile tests yield higher strength classes than bending tests based on strength and stiffness characteristic values, when all parameters are evaluated, it was determined that similar strength classes are obtained in tensile and bending tests. In this context, flatwise bending can be considered as an alternative to tensile and edgewise tests when determining strength classes, as they require a smaller sample size.

ACKNOWLEDGMENTS

Author Contributions

Availability of Data and Material

Data used for this work are available from the corresponding author upon reasonable request.

REFERENCES CITED

Arriaga, F., Iniguez-González, G., Esteban, M., and Divos, F. (2012). "Vibration method for grading of large cross-section coniferous timber species," *Holzforschung* 66, 381-387. https://doi.org/10.1515/hf.2011.167

As, N., Goker, Y., and Dundar, T. (2006). "Effect of knots on the physical and mechanical properties of Scots pine," *Wood Research* 51(3), 51-58.

Brunetti, M., Burato, P., Cremonini, C., Negro, F., Nocetti, M., and Zanuttini, R. (2016). "Visual and machine grading of larch (*Larix decidua* Mill.) structural timber from the Italian Alps," *Materials and Structures* 49(7), 2681-2688. https://doi.org/10.1617/s11527-0150676-5

EN 338 (2020). "Structural timber - Strength classes," European Committee of Standardization, Brussels, Belgium.

EN 384:2016+A1 (2018). "Structural timber - Determination of characteristic values of mechanical properties and density," European Committee of Standardization, Brussels, Belgium.

EN 408:2010+A1 (2012). "Timber structures - Structural timber and glued laminated timber - Determination of some physical and mechanical properties," European Committee of Standardization, Brussels, Belgium.

EN 1309-3 (2018). "Round and sawn timber - method and measurement," European Committee of Standardization, Brussels, Belgium.

EN 1912:2012 (2024). "Structural timber - Strength classes - Assignment of visual grades and species," European Committee of Standardization, Brussels, Belgium.

EN 13183-1 (2002). "Moisture content of a piece of sawn timber - Part 1: Determination by oven dry method," European Committee of Standardization, Brussels, Belgium.

EN 13183-2 (2002). "Moisture content of a piece of sawn timber - Part 2: Estimation by electrical resistance method," European Committee of Standardization, Brussels, Belgium.

EN 14080 (2013). "Timber structures – Glued laminated timber and glued solid timber – Requirements," European Committee of Standardization, Brussels, Belgium.

EN 14081-1-2016+A1 (2019). "Timber structures – Strength graded structural timber with rectangular cross section Part 1: General requirements," European Committee of Standardization, Brussels, Belgium.

EN 14081-2 (2018). "Timber structures – Strength graded structural timber with rectangular cross section Part 2: Machine grading; additional requirements for type testing," European Committee of Standardization, Brussels, Belgium.

EN 14358 (2016). "Timber structures - Calculation and verification of characteristic values," European Committee of Standardization, Brussels, Belgium.

Fernández-Golfín Seco, J. I., Diez Barra, M. R., Hermoso Prieto, E., and Conde García, M. (2004). "Mechanical characterization of timber from Spanish provenances of

laricio pine according to European standards," *Wood Science and Technology* 38(1), 25-34. https://doi.org/10.1007/s00226-003-0215-3

Fink, G., and Kohler, J. (2011). "Multiscale variability of stiffness properties of timber boards," in: *ICASP Applications of Statistics and Probability in Civil Engineering*, Taylor and Francis Group, Zurich, Switzerland, pp. 1369-1376.

Gil-Moreno, D., Ridley-Ellis, D., O'Ceallaigh, C., and Harte, A. M. (2022). "The relationship between bending and tension strength of Irish and UK spruce and pine," *European Journal of Wood and Wood Products* 80(3), 585-596. https://doi.org/10.1007/s00107-022-01787-6

Guindos, P., and Guaita, M. (2014). "The analytical influence of all types of knots on bending," *Wood Science and Technology* 48(3), 533-552. https://doi.org/10.1007/s00226-014-0621-8

ISO 13061-3 (2014). "Physical and mechanical properties of wood – Test methods for small clear wood specimens – Part 3: Determination of ultimate strength in static bending," International Organization for Standardization, Geneva, Switzerland.

ISO 13061-4 (2014). "Physical and mechanical properties of wood – Test methods for small clear wood specimens – Part 4: Determination of modulus of elasticity in static bending," International Organization for Standardization, Geneva, Switzerland.

Krajnc, L., Farrelly, N., and Harte, A. M. (2019). "Relationships between wood properties of small clear specimens and structural-sized boards in three softwood species," *Holzforschung* 73(11), 987-996. https://doi.org/10.1515/hf-2019-0039

Kurul, F. (2025). "Göknar ve karaçam tahtalarının TS 1265 standardına göre görsel mukavemet sınıflandırması [Visual strength classification of fir and larch wood according to TS 1265 standard]," *Anadolu Orman Araştırmaları Dergisi* 11(1), 162-167. https://doi.org/10.53516/ajfr.1675730

Kurul, F., and As, N. (2024). "Visual and machine strength gradings of Scots and red pine structural timber pieces from Türkiye," *BioResources* 19(3), 4135-4154. https://doi.org/10.15376/biores.19.3.4135-4154

Kurul, F., Görgün, H. V., Şeker, S., Yılmaz, T., Dündar, T., and Ayrilmis, N. (2025). "Experimental and numerical modeling of bending characteristics of fir and black pine wood from different forest regions in Türkiye," *Forests* 16(5), article 844. https://doi.org/10.3390/f16050844

Kurul, F., Şişman, Ö. A., and Dündar, T. (2024). "Mechanical characterization of visually graded boards from Turkish fir and black pine by nondestructive and destructive tests," *Maderas. Ciencia y Tecnología* 26. https://doi.org/10.22320/s0718221x/2024.17

Lovrić Vranković, J., Uzelac Glavinić, I., Boko, I., and Torić, N. (2025). "An experimental investigation on the tensile properties parallel to the grain of European hornbeam (*Carpinus betulus* L.) boards," *European Journal of Wood and Wood Products* 83(4), article 130. https://doi.org/10.1007/s00107-025-02286-0

Montero, M., De la Mata, J., Esteban, M., and Hermoso, E. (2015). "Influence of moisture content on the wave velocity to estimate the mechanical properties of large cross-section pieces for structural use of Scots pine from Spain," *Maderas. Ciencia y Tecnología* 17(2), 407-420. https://doi.org/10.4067/S0718-221X2015005000038

Nocetti, M., Bacher, M., Brunetti, M., Crivellaro, A., and Van De Kuilen, J. W. G. (2010). "Machine grading of Italian structural timber: preliminary results on different wood species," *Proceedings of the World Conference on Timber Engineering (WCTE)*, Riva del Garda, Italy, pp. 8-14.

Qu, H., Chen, M., Hu, Y., and Lyu, J. (2020). "Effect of trees knot defects on wood quality: A review," *IOP Conference Series: Materials Science and Engineering* 738, article 012027. https://doi.org/10.1088/1757-899X/738/1/012027

Rais, A., Bacher, M., Khaloian-Sarnaghi, A., Zeilhofer, M., Kovryga, A., Fontanini, F., Hilmers, T., Westermayr, M., Jacobs, M., Pretzsch, H., *et al.* (2021). "Local 3D fibre orientation for tensile strength prediction of European beech timber," *Construction and Building Materials* 279(11), article 122527. https://doi.org/10.1016/j.conbuildmat.2021.122527

Ravenshorst, G. J. P., and Van de Kuilen, J. W. G. (2016). "A new approach for the derivation of settings for machine graded timber," *Wood Material Science & Engineering*, 11(2), 79-94. https://doi.org/10.1080/17480272.2014.950329

Ridley-Ellis, D., Stapel, P., and Baño, V. (2016). "Strength grading of sawn timber in Europe: an explanation for engineers and researchers," *European Journal of Wood and Wood Products* 74(3), 291-306. https://doi.org/10.1007/s00107-016-1034-1

Roblot, G., Bléron, L., Mériaudeau, F., and Marchal, R. (2010). "Automatic computation of the knot area ratio for machine strength grading of Douglas-fir and Spruce timber," *European Journal of Environmental and Civil Engineering* 14(10), 1317-1332. https://doi.org/10.1080/19648189.2010.9693296

Stapel, P., and van de Kuilen, J.-W. G. (2013). "Influence of cross-section and knot assessment on the strength of visually graded Norway spruce," *Eur. J. Wood Prod.* 72:213–227. https://doi.org/10.1007/s00107-013-0771-7

Stapel, P., and van de Kuilen, J.-W. G. (2014). "Efficiency of visual strength grading of timber with respect to origin, species, cross section, and grading rules: A critical evaluation of the common standards," *Holzforschung* 68(2), 203-216. https://doi.org/10.1007/s00107-013-0771-7

Steiger, R., and Arnold, M. (2009). "Strength grading of Norway spruce structural timber: Revisiting property relationships used in EN 338 classification system," *Wood Science and Technology* 43, 259-278. https://doi.org/10.1007/s00226-008-0221-6

TS 1265 (2012). "Sawn timber (Coniferous) - For building construction," Turkish Standards Institute, Ankara, Turkey.

Article submitted: October 18, 2025; Peer review completed: November 22, 2025; Revised version received: November 23, 2025; Accepted: December 15, 2025; Published: December 26, 2025.
DOI: 10.15376/biores.21.1.1364-1387